

Search for charge nonconservation and Pauli exclusion principle violation with the MAJORANA DEMONSTRATOR

I.J. Arnquist,¹ F.T. Avignone III,^{2,3} A.S. Barabash,⁴ C.J. Barton,⁵ K.H. Bhimani,^{6,7} E. Blalock,^{8,7} B. Bos,^{6,7} M. Busch,^{9,7} M. Buuck,^{10, a} T.S. Caldwell,^{6,7} Y-D. Chan,¹¹ C.D. Christofferson,¹² P.-H. Chu,¹³ M.L. Clark,^{6,7} C. Cuesta,¹⁴ J.A. Detwiler,¹⁰ Yu. Efremenko,^{15,3} H. Ejiri,¹⁶ S.R. Elliott,¹³ G.K. Giovanetti,¹⁷ M.P. Green,^{8,7,3} J. Gruszko,^{6,7} I.S. Guinn,^{6,7} V.E. Guiseppe,³ C.R. Haufe,^{6,7} R. Henning,^{6,7} D. Hervas Aguilar,^{6,7} E.W. Hoppe,¹ A. Hostiuc,¹⁰ M.F. Kidd,¹⁸ I. Kim,^{13, b} R.T. Kouzes,¹ T.E. Lannen V,² A. Li,^{6,7} J.M. López-Castaño,^{3, c} E.L. Martin,^{6,7, d} R.D. Martin,¹⁹ R. Massarczyk,¹³ S.J. Meijer,¹³ T.K. Oli,⁵ L.S. Paudel,⁵ W. Pettus,^{20,21} A.W.P. Poon,¹¹ D.C. Radford,³ A.L. Reine,^{6,7} K. Rielage,¹³ N.W. Ruof,¹⁰ D.C. Schaper,¹³ D. Tedeschi,² R.L. Varner,³ S. Vasilyev,²² J.F. Wilkerson,^{6,7,3} C. Wiseman,^{10, e} W. Xu,⁵ C.-H. Yu,³ and B.X. Zhu^{13, f}

(MAJORANA Collaboration)

¹*Pacific Northwest National Laboratory, Richland, WA 99354, USA*

²*Department of Physics and Astronomy, University of South Carolina, Columbia, SC 29208, USA*

³*Oak Ridge National Laboratory, Oak Ridge, TN 37830, USA*

⁴*National Research Center “Kurchatov Institute” Institute for Theoretical and Experimental Physics, Moscow, 117218 Russia*

⁵*Department of Physics, University of South Dakota, Vermillion, SD 57069, USA*

⁶*Department of Physics and Astronomy, University of North Carolina, Chapel Hill, NC 27514, USA*

⁷*Triangle Universities Nuclear Laboratory, Durham, NC 27708, USA*

⁸*Department of Physics, North Carolina State University, Raleigh, NC 27695, USA*

⁹*Department of Physics, Duke University, Durham, NC 27708, USA*

¹⁰*Center for Experimental Nuclear Physics and Astrophysics, and*

Department of Physics, University of Washington, Seattle, WA 98195, USA

¹¹*Nuclear Science Division, Lawrence Berkeley National Laboratory, Berkeley, CA 94720, USA*

¹²*South Dakota Mines, Rapid City, SD 57701, USA*

¹³*Los Alamos National Laboratory, Los Alamos, NM 87545, USA*

¹⁴*Centro de Investigaciones Energéticas, Medioambientales y Tecnológicas, CIEMAT 28040, Madrid, Spain*

¹⁵*Department of Physics and Astronomy, University of Tennessee, Knoxville, TN 37916, USA*

¹⁶*Research Center for Nuclear Physics, Osaka University, Ibaraki, Osaka 567-0047, Japan*

¹⁷*Physics Department, Williams College, Williamstown, MA 01267, USA*

¹⁸*Tennessee Tech University, Cookeville, TN 38505, USA*

¹⁹*Department of Physics, Engineering Physics and Astronomy, Queen’s University, Kingston, ON K7L 3N6, Canada*

²⁰*Department of Physics, Indiana University, Bloomington, IN 47405, USA*

²¹*IU Center for Exploration of Energy and Matter, Bloomington, IN 47408, USA*

²²*Joint Institute for Nuclear Research, Dubna, 141980 Russia*

(Dated: January 12, 2023)

Charge conservation and the Pauli exclusion principle (PEP) result from fundamental symmetries in the Standard Model, and are typically taken as axiomatic. High-precision tests for small violations of these symmetries could point to new physics. In this work we consider three models for violation of these processes which would produce detectable ionization in the high-purity germanium detectors of the MAJORANA DEMONSTRATOR. Using a 37.5 kg-yr exposure, we report a new lower limit on the electron mean lifetime of $\tau_e > 3.2 \times 10^{25}$ yr (90% CL), the best result for this decay channel ($e \rightarrow \nu_e \bar{\nu}_e \nu_e$ or more generally $e \rightarrow$ invisibles) in more than two decades. We also present searches for two types of violation of the PEP, setting new limits on the probability of two electrons forming a symmetric quantum state. Using our ²²⁸Th calibration data set, which introduces electrons new to the system through electron-positron pair production, we obtain a world-leading model-independent limit for a terrestrial experiment of $\beta^2/2 < 1.0 \times 10^{-3}$ (99.7% CL). Our 37.5 kg-yr exposure is also used to search for a process where an electron in an atomic system spontaneously violates the PEP, resulting in a model-dependent upper limit of $\beta^2/2 < 1.0 \times 10^{-48}$ (90% CL).

Searches for small violations of fundamental symmetries have driven modern experimental physics, from the discovery of parity nonconservation in β -decay [1], to tests disproving Bell’s inequality [2–4]. In this work we consider two well-validated principles of quantum mechanics, charge conservation and Pauli exclusion, which emerge from robust mathematical frameworks and are

typically taken as axioms. Many models have been proposed which allow their violation by exotic mechanisms [5–13], and point to signs of new physics.

Large underground radiation detectors offer a novel environment to search for rare signals produced by such symmetry violations. The MAJORANA DEMONSTRATOR, a high-purity germanium (HPGe) array, has world-

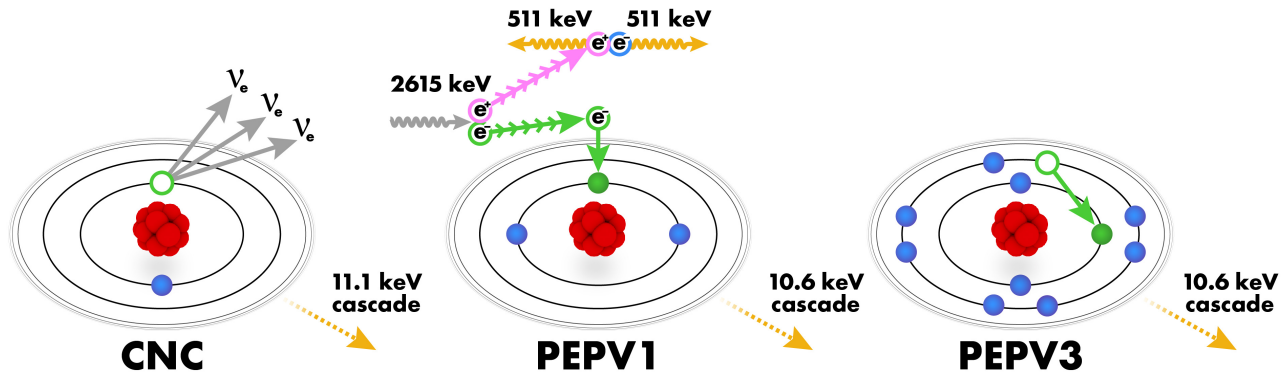


FIG. 1. Three processes disallowed by quantum mechanics that would produce ionization in Ge atoms. A simplified view of the atom includes a nucleus (red) surrounded by the closest orbital electrons (blue) depicting their nonstandard processes (green). Additional bound electrons are not illustrated for clarity. *Left*: Charge nonconservation, with an electron decaying to three neutrinos. *Middle*: Pauli exclusion principle (PEP) violation by a newly born electron produced by pair production from an incident gamma (Type I) *Right*: PEP violation where an electron descends to a fully occupied energy level (Type III).

leading energy resolution and ultra-low levels of radioactive backgrounds, and in addition to its primary search for neutrinoless double beta decay [14, 15], it has been used to search for bosonic dark matter [16, 17], fractionally charged particles [18], trinucleon decay [19], and signatures of quantum wavefunction collapse [20].

The DEMONSTRATOR consists of two separate modules of p-type point contact (PPC) HPGe detectors, with 29.7 kg enriched in ^{76}Ge , and collected an ultimate exposure of 65 kg-yr [15]. From this primary data set, an exposure of 37.5 kg-yr of $^{\text{enr}}\text{Ge}$ data was selected for analysis of the 1–100 keV low-energy range. To produce the final spectrum, a series of analysis cuts are applied which remove events from electronics noise and energy-degraded surface events, while retaining bulk events above 20 keV with 92% efficiency [17]. The $^{\text{enr}}\text{Ge}$ detectors achieved background rates of 0.01 counts/(keV kg d) from 20–40 keV and 0.06 counts/(keV kg d) at 5 keV through use of highly radiopure materials, the deep underground location, and careful control of the surface exposure time. In the spectrum, we observe a nearly flat continuum consisting of Compton scatter events between 20–100 keV, with contributions from ^3H , ^{55}Fe , and ^{68}Ge below 20 keV.

In this work, we present an experimental test of charge conservation, searching for the spontaneous disappearance of an electron to “invisibles” (no photons), with the most favorable mode being to three neutrinos, ($e \rightarrow \nu_e \bar{\nu}_e \nu_e$) [21]. Our result for the mean lifetime of the electron is the best in more than two decades [22]. We then report new limits on violations of the Pauli exclusion principle, which would also have a detectable ionization signature in our HPGe array. These “forbidden” mechanisms considered are illustrated in Fig. 1.

I. TEST OF ELECTRIC CHARGE CONSERVATION

Conservation of electric charge arises from the global U(1) symmetry gauge invariance of the electric field [23]. The photon is the associated gauge boson, massless and exactly symmetric under gauge transformation with an unobservable quantum phase. Extremely small experimental upper limits on the photon mass are generally considered to be evidence of exact electric charge conservation. However, there are theoretical BSM frameworks which allow electric charge nonconservation, either by broken gauge symmetry or by hidden processes such as charge leakage into extra dimensions [24–27].

Violation of charge conservation implies that electrons, the lightest charged leptons, may have a finite lifetime. Hence, the conservation of electric charge can be tested by searching for the decay of electrons to chargeless particles with lighter mass, such as neutrinos and photons. Experiments have set limits on the decay process ($e \rightarrow \nu_e \gamma$) by searching for a peak at 255.5 keV, with the best result from Borexino giving a mean lifetime $\tau_e > 6.6 \times 10^{28}$ y [28]. The electron may also decay without a photon to multiple neutrinos or other unknown chargeless BSM particles, often referred to as a “disappearance” mode. Decay to three neutrinos ($e \rightarrow \nu_e \bar{\nu}_e \nu_e$) is considered the most favorable of these modes, being comprised of known particles which can balance angular momentum and conserve lepton number. In general, a search for electron disappearance would include effects from any “invisible” mechanism, not only the three-neutrino mode. Disappearance mechanisms to date give lifetimes on the order of 10^{24} years [21], and we point out that if more than one decay mode is available for an electron, the channel with the shorter lifetime will be favored.

Data from the low-background physics run of the

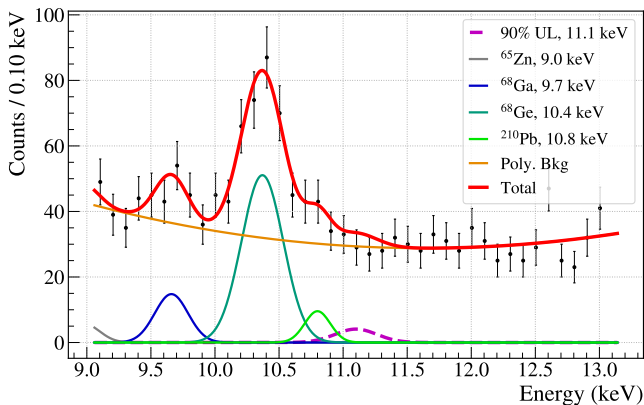


FIG. 2. Spectral fit of the energy region surrounding the peak at 11.1 keV expected from the $(e \rightarrow \nu_e \bar{\nu}_e \nu_e)$ charge nonconserving decay of a Ge K-shell electron. The 90% CL upper limit on the rate is $R = 0.0013$ counts/kg-d, taken from a 37.5 kg-y exposure.

DEMONSTRATOR can be used to search for decay of atomic electrons within the HPGe detectors. If a K-shell (ground state) electron in a Ge atom decays to neutrinos (or other invisibles), a hole is produced in the shell, and electrons in higher shells will cascade to fill it, emitting X-rays and Auger electrons until the full binding energy (11.1 keV) is released. This cascade occurs in a short time scale relative to the HPGe charge collection time, making the signature of this process a Gaussian peak in the spectrum at 11.1 keV.

We perform an unbinned maximum likelihood fit in the region of interest, and extract an upper limit on the potential contribution from an absent peak by varying the number of counts in the peak and profiling the likelihood function to a particular confidence level (90%, 95%, or 99%) to compare with previous literature values. The excellent energy resolution allows discrimination from the nearby 10.37 keV X-ray line originating from ^{68}Ge electron capture decay, and the acceptance efficiency of the pulse shape analysis cuts is $(91 \pm 2)\%$ at 11.1 keV. The energy calibration provided by the $\beta\beta(0\nu)$ analysis is validated by observation of the 10.37 keV line at the expected energy. The background function is a second-order Chebyshev polynomial, and nearby cosmogenic peaks are included in the model. This method is the same one used to search for peaked signatures for exotic dark matter in Ref. [17] and further details are given in Sec. A. The fit result is shown in Fig. 2, giving a 90% upper limit on the event rate at 11.1 keV of $R = 0.0013$ counts/(kg-d). The limit on the mean lifetime $\tau_e = n_e/R$ is calculated from the upper limit on the decay rate per unit time R , the number density of Ge atoms, $N_{\text{Ge}} = 7.96 \times 10^{24}/\text{kg}$, and two K-shell electrons for each Ge atom, $n_e = 2N_{\text{Ge}}$. We find a mean lifetime of $\tau_e(e \rightarrow \nu_e \bar{\nu}_e \nu_e) > 3.2 \times 10^{25}$ y at 90% CL, the most stringent limit for this decay channel by a factor 13 over Ref. [22].

II. TESTS OF PAULI EXCLUSION PRINCIPLE VIOLATION

The Pauli exclusion principle (PEP) states that two identical fermions cannot occupy the same quantum state [29]. In modern quantum mechanics, it is understood to originate from the spin-statistics theorem, which describes the antisymmetric behavior of fermions in quantum systems [30]. Many mechanisms of PEP-violation have been proposed, making a direct comparison difficult [8, 9, 31–34]. Experimental tests of the PEP may set limits on the probability of two fermions to form a *symmetric* quantum state. In this work it is taken to be a ratio of lifetimes between PEP-obeying (antisymmetric) and PEP-violating (symmetric) atomic transitions of electrons,

$$\beta^2/2 \equiv \tau_{\text{PEP}}/\tau_{\text{PEP-V}}. \quad (1)$$

The transitions in which a model allows the PEP to be violated are determined by the initial symmetric states of the electron. In particular, the Messiah-Greenberg superselection rule [35] forbids transitions of individual electrons between antisymmetric and symmetric states, allowing only newly created electrons, or electrons already in a symmetric state, to make the transition. As electrons in symmetric states have not been observed, the newly created ones are the only model-independent test currently available. This constraint, however, can be evaded by exotic physics such as the existence of extra dimensions or electron substructure [36, 37]. More recently, it has been proposed that the violation of the spin-statistics theorem and hence PEP violation can emerge naturally from quantum gravity [38]. The paper by Elliott et al. [39] reviews the experimental and theoretical considerations. Following this framework, processes that can violate the PEP are classified into three categories:

- **Type I** interactions are between a system of electrons and a PEP-violating electron that has not previously interacted with other electrons. A newly created electron from pair production has not established previous symmetry with any system, and a PEP-violating process is allowed by any model. It can travel a short distance between atoms before interacting with (or being captured by) an atomic shell.
- **Type II** interactions are between a system of electrons and an electron that has not previously interacted with that given system. An electron may be created (or already exist in a steady state), travel some distance, and interact with another system such as an atom, e.g. through an electric current, with some probability of PEP violation.
- **Type III** interactions are between a system of electrons and an electron within that given system. This is the most model-dependent search, since the

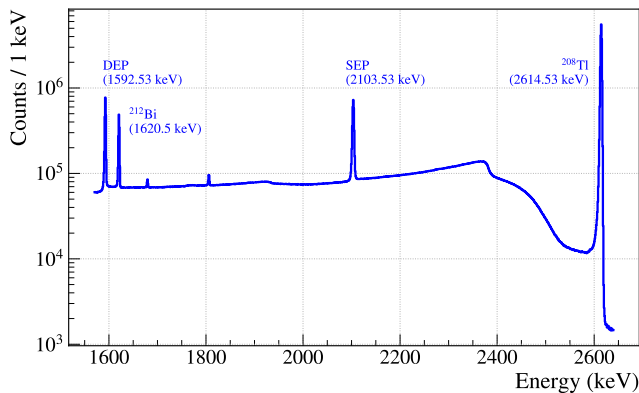


FIG. 3. The combined ^{228}Th spectrum for all active detectors in the MAJORANA DEMONSTRATOR calibration data set, from data taken during 2015–2019.

PEP-violating electron is already in a steady state in its host atom.

Each type of PEP violation can be tested experimentally with HPGe detectors, and tests of Types I and III are possible with the DEMONSTRATOR data set. A Type I search is performed using the ^{228}Th calibration data, and a Type III search is performed with the 37.5 kg-yr low-energy background data. A Type II search has been done previously in Ref. [39] with a prototype MAJORANA detector, using electrical current through Pb as the transition source, and more recently the VIP-2 experiment has improved this limit [40, 41]. We note that in the final state, a PEP-violating electron could in principle persist in the K shell indefinitely, which would change the chemical properties of the atom and be detectable by spectroscopic methods [42]. Ref. [39] considers these long-lived final states unlikely, and the PEP-violating electron could subsequently decay (e.g. to three neutrinos).

A. Type I PEP Violation: Electrons generated by pair production in ^{228}Th calibration data

The calibration system of the DEMONSTRATOR consists of twin ^{228}Th line sources, periodically introduced into the system for weekly 60-90 minute calibrations of each module and periodic longer runs. We utilize 40.43 days from the first detector module, and 21.38 days from the second module. The signature of Type I PEP violation in the MAJORANA calibration data set can be observed from pair production events produced by 2614.5 keV gamma rays from the decay of ^{208}Tl in the ^{228}Th line source (Fig. 1), which create electron-positron pairs in the detectors. The positron annihilation produces two 511.0 keV gamma rays, and one or both may escape the detector, creating single-escape peak (SEP) events at 2103.5 keV and double-escape peak (DEP) events at 1592.5 keV. If the PEP is violated, the pair-produced electron may be captured by a Ge atom and

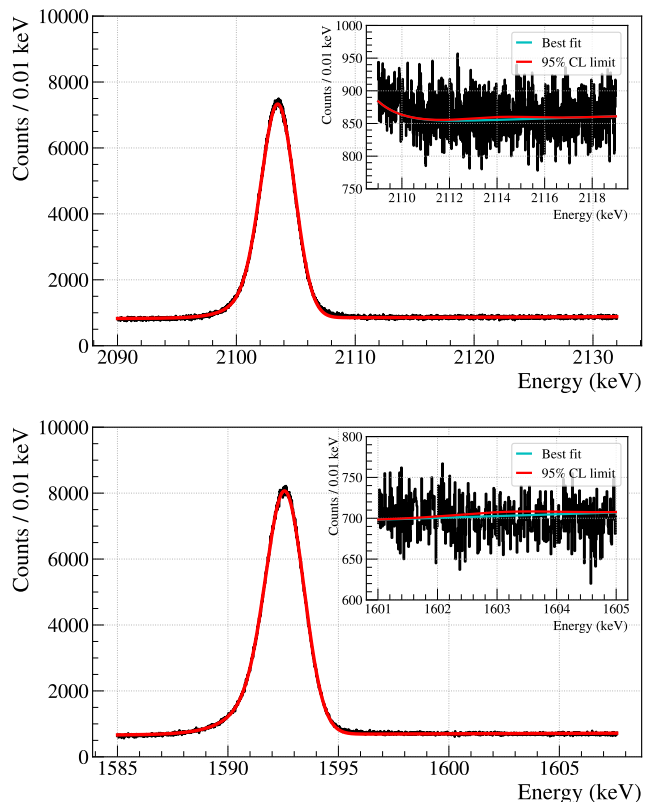


FIG. 4. Calibration fits in the single-escape peak (SEP, top) and double-escape peak (DEP, bottom) regions, showing the best-fit from the combined fit of the SEP and DEP peaks (cyan), and the contribution to the 10.6 keV region above the peak corresponding to a 95% CL upper limit on $\beta^2/2$ (red).

transition to the already occupied K shell. The transition energy of this forbidden process and the cascade of electrons to fill the empty L-shell will add up to release 10.6 keV of energy, when correcting for the additional shielding of the nuclear charge when the K shell is occupied [39]. The full-energy peak contains a significant contribution of ionization events with no pair production, which precludes its use in our search. The additional cascade produced by the PEP-violating capture to the K shell sums with the SEP or DEP energy, making the signature of the transition a peak 10.6 keV above the SEP and DEP peaks. The best prior limit for this process is $\beta^2/2 < 1.4 \times 10^{-3}$ (3σ CL) [39] achieved by using a single HPGe detector and ^{228}Th source. Our calibration runtime and active detector mass are both significantly larger, comprising a multi-year run of the DEMONSTRATOR. The spectrum used for our Type I search is shown in Fig. 3, with standard data cleaning and quality cuts applied [43].

Analysis of the peaks 10.6 keV above the SEP (2104 keV) and DEP (1592 keV) peak can be done separately or with a combined fit. Since $\beta^2/2$ is defined in terms of the ratio $\tau_{\text{PEP}}/\tau_{\text{PEP-V}}$, many systematics including uncertainties in efficiency and exposure cancel

TABLE I. Upper limits on $\beta^2/2$ from each fit technique, with the combined fit method giving the most stringent limit.

method	95% CL	3σ (99.7%) CL
SEP + DEP	6.3×10^{-4}	1.0×10^{-3}
SEP	1.3×10^{-3}	1.6×10^{-3}
DEP	1.6×10^{-3}	2.1×10^{-3}

out, resulting in a more robust search. For each detection method, we employ a binned likelihood fit approach adapted to a variable binning, to reduce statistical and systematic errors associated with each peak. The SEP and DEP are fit with a precision peakshape function to reduce systematic error [43], while the PEP-violating peak 10.6 keV above is counted using a single bin to minimize statistical error and measure the rate only. The primary peak is selected to compute an upper limit on τ_{PEP} , and the upper region gives $\tau_{\text{PEP-v}}$. This allows us to compute the lifetimes τ_{PEP} and $\tau_{\text{PEP-v}}$ and set limits on $\beta^2/2$, by performing a simple counting analysis of the events in each peak.

The sensitivity of the three detection techniques depends on the signal peak and background count rates at each energy, and the results from each method are given in Table I and Fig. 4. Our most stringent result is obtained from a combined fit of the SEP+DEP regions of interest, $\beta^2/2 < 1.0 \times 10^{-3}$ at 99.7% CL (3σ). This is currently the best of all terrestrial Type I PEP violation searches, improving the previous best limit by 30%.

B. Type III PEP Violation: Electron transition in low-energy background data

We also searched for Type-III PEP-violating transition of an L-shell electron in a Ge atom to the already occupied K-shell [10, 16], shown in Fig. 1. The signature of this process is a Gaussian peak at 10.6 keV, which would appear as a shoulder on the 10.37 keV ^{68}Ge peak. Similar to the CNC search, we search for the PEP-violating atomic transition with the 37.5 kg-yr low-energy data set. The total efficiency of the low-energy cuts is $(91 \pm 2)\%$ at 10.6 keV, and we set an upper limit of the count rate in the spectrum at the region of interest with the same profile likelihood technique.

We find an upper limit on the count rate at 10.6 keV, $R = 0.0041$ counts/kg-d (90% CL), shown in Fig. 5. We then calculate the mean lifetime using the same expression for lifetime as in Sec. II A, $\tau_e = n_{\text{Ge}}/R$. We find a mean lifetime of 1.7×10^{32} s (90% CL). MAJORANA previously set the most stringent upper limit at 90% CL on this process, at $\beta^2/2 < 8.5 \times 10^{-48}$ with 478 kg-d exposure [16]. Comparing to the 1.7×10^{-16} s mean lifetime of a standard K- α transition in Ge, we set an improved limit on the PEP-violating transition at $\beta^2/2 < 1.0 \times 10^{-48}$ (90% CL), a factor 8.9 improvement over the previous limit [16].

C. Discussion

Low-background underground radiation detectors offer a unique environment to search for weak signatures from nonstandard processes. This work is an important complement to searches such as VIP-2 [40, 41], which search for Type-II PEP-violation by circulating large numbers of charge carriers through a sensitive detection volume. Larger Ge arrays with lower backgrounds are currently in active development [44] and an order-of-magnitude improvement in these tests of fundamental quantum mechanical principles may soon be attained.

ACKNOWLEDGMENTS

This material is based upon work supported by the U.S. Department of Energy, Office of Science, Office of Nuclear Physics under contract / award numbers DE-AC02-05CH11231, DE-AC05-00OR22725, DE-AC05-76RL0130, DE-FG02-97ER41020, DE-FG02-97ER41033, DE-FG02-97ER41041, DE-SC0012612, DE-SC0014445, DE-SC0018060, DE-SC0022339, and LAN-LEM77/LANLEM78. We acknowledge support from the Particle Astrophysics Program and Nuclear Physics Program of the National Science Foundation through grant numbers MRI-0923142, PHY-1003399, PHY-1102292, PHY-1206314, PHY-1614611, PHY-1812409, PHY-1812356, PHY-2111140, and PHY-2209530. We gratefully acknowledge the support of the Laboratory Directed Research & Development (LDRD) program at Lawrence Berkeley National Laboratory for this work. We gratefully acknowledge the support of the U.S. Department of Energy through the Los Alamos National Laboratory LDRD Program and through the Pacific Northwest National Laboratory LDRD Program for this work. We gratefully acknowledge the support of the South Dakota Board of Regents Competitive Research Grant. We acknowledge the support of the Natural Sciences and Engineering Research Council of Canada, funding reference number SAPIN-2017-00023, and from the Canada Foundation for Innovation John R. Evans Leaders Fund. This research used resources provided by the Oak Ridge Leadership Computing Facility at Oak Ridge National Laboratory and by the National Energy Research Scientific Computing Center at Lawrence Berkeley National Laboratory, a U.S. Department of Energy Office of Science User Facility. We thank our hosts and colleagues at the Sanford Underground Research Facility for their support.

Appendix A: Methods

1. Detectors and data taking scheme

The DEMONSTRATOR was located at the 4850-ft underground of the Sanford Underground Research Facility.

ity (SURF) in Lead, South Dakota, consisting of two separate ultra-low background modules of PPC HPGe detectors with a total mass of 44.1 kg, of which 29.7 kg were enriched to 88% in ^{76}Ge [45]. The detectors were operated in a vacuum cryostat within a graded shield made from ultra-low background electroformed Cu and other shielding materials sourced to meet stringent material purity requirements [46].

The DEMONSTRATOR calibration system accommodates a ^{228}Th line source through a track penetrating the shield and surrounding each cryostat in a helical shape [47]. When deployed, the line source exposed all detectors in the array for energy calibration and stability determination. During normal operations, sources were deployed weekly for 60–90 minutes to perform routine energy calibrations, while longer runs (12–24 hours) were taken to refine energy and other pulse shape analysis parameters.

From 2015–2019 the original set of 35 $^{\text{enr}}\text{Ge}$ detectors were operated, using a data blindness scheme of alternating 31 hours of open data followed by 93 hours of blinded data, to mitigate possible bias in the development of analysis routines. Analysis of the calibration data set does not employ a blinded approach. The DEMONSTRATOR continues to operate with 14.3 kg of natural Ge detectors in a single module for background studies and other rare-event searches.

2. Peak fits at low energy

The peak scanning algorithm uses a $\pm(7\sigma_{\text{res}} + 1)$ keV window near the peak position as the fit region of interest (ROI), where σ_{res} is the exposure-weighted combined detector resolution as a function of energy. The 1 keV offset ensures an ROI of at least 2 keV, even for a vanishingly small σ . The ROI for the PEP-violating transition search at 10.6 keV is 8.6–12.6 keV, and the ROI for the charge nonconserving electron decay at 11.1 keV is 9.1–13.2 keV. In the low-energy background data near the 10.6 keV signature, cosmogenic peaks at ^{65}Zn (8.98 keV), ^{68}Ga (9.66 keV), and ^{68}Ge (10.37 keV) are expected. External ^{210}Pb may also induce a peak at 10.8 keV. The energy calibration in the low-energy region is precise enough to treat the location of the cosmogenic peaks as fixed at the literature values. Other contributions from tritium beta decay and Compton scattering from higher energy peaks form a background continuum that is separable from the peak-like signature, and is approximated by a second-order polynomial within the ROIs.

In the narrow ROIs where the background continuum can be approximated as a second-order polynomial, the spectrum is modeled as

$$\mathcal{P}(E; \theta) = \eta(E) \left(n_0 \mathcal{P}_{\text{poly}} + \sum_i^{n_{\text{pks}}} n_i \mathcal{P}_{G,i} + n_{\text{obs}} \mathcal{P}_{\text{rare}} \right), \quad (\text{A1})$$

where $\mathcal{P}_{\text{poly}}$, $\mathcal{P}_{G,i}$ and $\mathcal{P}_{\text{rare}}$ are the normalized spectral distributions for the polynomial background, i -th cosmo-

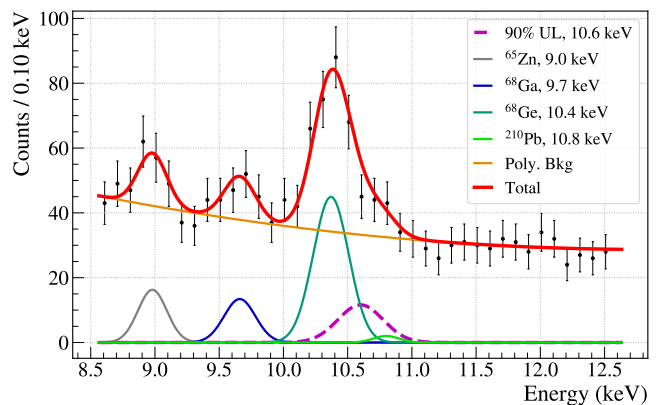


FIG. 5. The 90% CL spectral fit of the rare Gaussian peak at 10.6 keV expected from the PEP-violating transition of an L-shell electron in a Ge atom to the already-occupied K-shell. The 90% CL upper limit on the counts at 10.6 keV is 0.0041 counts/kg-d.

genic peak and the rare event peak of interest, respectively, and n_0 , n_i and n_{obs} are the number of events in each distribution. Additional nuisance parameters are denoted θ . We fit the model spectrum to the data using the unbinned extended likelihood method [48–50]. While the shape parameters for the polynomial background are unbounded, the widths of the Gaussian rare peak and background peaks are constrained by the detector energy resolution.

Profiling the likelihood function by varying the number of counts in the rare signal peak, and fixing all other nuisance parameters at their best-fit values, is a standard technique which results in a conservative upper limit on the rate. The signal peaks in both the CNC and Type III PEP searches overlap to some extent with the cosmogenic lines. The likelihood contour is typically flat up to the number of counts assigned to the overlapping peaks, and only increases to the desired CL above these counts; hence the presence of overlapping peaks does not result in an artificially better limit. Fig. 5 shows the spectral fit in the ROI of the PEP-violating atomic transition in Ge at the 90% CL upper limit.

The total acceptance efficiency $\eta(E)$ of the low-energy data cleaning cuts is determined by convolving the data cleaning efficiency, the individual detector threshold efficiencies, and the efficiency of the energy-degraded slow pulse event rejection [51]. The low-energy cuts retain $(91 \pm 2)\%$ of single-site events in our ROI, which we take to be constant within each narrow fit window. We note that the efficiency correction is a smooth function and will not introduce peak structures, and remains above 80% acceptance down to 3 keV [17]. A complementary search for the signature of a PEP-violating transition to the L-shell (~ 1.3 keV) may be undertaken, but would produce a weaker signal and less well-motivated result.

3. Peak fits at high energy

Our search for the peaks 10.6 keV above the single- and double-escape peaks, and resulting limit, uses a binned profile likelihood analysis method. The PEP-violating peak is expected to be very faint, and in this analysis we refer to this region as the “echo” peak. Initial values for the SEP and DEP parameters are obtained from a fit to each peak, and are input to the main fit containing both the escape and echo peak regions. The PEP-violating parameter $\beta^2/2$ is defined by the ratio of lifetimes, $\tau_{\text{PEP}}/\tau_{\text{PEP-v}}$, and is obtained from the ratio of counts in each peak region of interest,

$$\frac{\beta^2}{2} = \frac{N_{\text{echo}}}{N_{\text{peak}}} = \frac{N_{\text{echo,SEP}} + N_{\text{echo,DEP}}}{N_{\text{peak,SEP}} + N_{\text{peak,DEP}}}. \quad (\text{A2})$$

We maximize the sensitivity by considering counts from both the SEP and DEP regions, as shown by Table I.

Our signal model consists of contributions from the two peaks $\mathcal{P}_{\text{peak}}$, $\mathcal{P}_{\text{echo}}$, which we write as a cumulative distribution function over energy E with nuisance parameters θ and bin index i :

$$\begin{aligned} \mathcal{C}_i(\beta, \theta) = & N_{\text{peak}} \int_i \mathcal{P}_{\text{peak}}(E, \theta) dE \\ & + \frac{\beta^2}{2} N_{\text{echo}} \int_i \mathcal{P}_{\text{echo}}(i). \end{aligned} \quad (\text{A3})$$

We precisely measure the escape peak counts with a precision peakshape function $\mathcal{P}_{\text{peak}}$, and combine all counts in the echo peak $\mathcal{P}_{\text{echo}}$ into a single bin with width $5\sigma_{\text{res}}$. A multi-bin peak fit is not optimal for a faint (or nonexistent) bump, since its shape is completely hidden within the Poisson uncertainty of the background. The energy regions selected for the DEP and SEP peaks are chosen where the Compton background can be accurately modeled by a linear term, avoiding one nearby gamma peak from ^{212}Bi at 1620 keV, and are given in Table II.

We fit the DEP and SEP peaks with a germanium peakshape $\mathcal{P}_{\text{peak}}$, comprised of the Ge response [43], a smoothed step function and linear background term, and an overall count normalization,

$$\begin{aligned} \mathcal{P}_{\text{peak}}(E, \theta) = & \frac{N_{\text{peak}} f}{2\lambda} \exp\left(\frac{\sigma_g^2}{2\lambda^2} - \frac{E-\mu}{\lambda}\right) \times \\ \text{erfc}\left(\frac{\sigma_g}{\sqrt{2}\lambda} - \frac{E-\mu}{\sqrt{2}\sigma_{\text{res}}}\right) + & H \text{erfc}\left(\frac{E-\mu}{\sigma_g}\right) + mE + n. \end{aligned} \quad (\text{A4})$$

The peakshape function is a sum of a Gaussian with several correction terms. At its mean energy μ , the Gaussian width σ_g is allowed to float from the expected resolution σ_{res} . The error function describes the low-energy tail, including an exponential slope λ and the fraction of signal events in the tail f . A smoothed step function contribution with height H is included to account for events which have undergone small-angle Compton scattering, losing energy and not contributing directly to the main

TABLE II. Energy range for fitting in the hit spectrum, energy range of the PEP-violating peak used as a single-bin in the likelihood fit, and bin size, chosen such that the Poisson uncertainty of each bin is less than 5%.

	SEP	DEP
Escape peak (keV)	[2090.0 – 2132.0]	[1585 – 1607.6]
Echo peak (keV)	[2110.1 – 2118.1]	[1599.9 – 1606.3]
Bin size (keV)	0.01	0.01

peak. The parameters m and n define the slope and floor of the linear background below the peak, respectively.

Grouping the nuisance parameters, we have

$$\theta = (N_{\text{peak}}, \mu, \sigma_g, f, H, m, n, \lambda). \quad (\text{A5})$$

Prior to fitting with the full peakshape in Eq. A4, the peaks are fit to a simple Gaussian and linear background to obtain initial values. The expected energy resolution σ_{res} is calculated by the primary $0\nu\beta\beta$ analysis using calibration data [15]. The other parameters in the peakshape function are set to initial values of $\lambda = 1.7$ keV, $f = 0.15$ and $H = 0$.

To search for the existence of the echo peak, and set an upper limit if its best-fit value is not significant, we construct a variable-width binned likelihood function \mathcal{L}_i based on the signal model \mathcal{C}_i . We use products of the Poisson probability of finding the observed number of events in bin i when the expected value is \mathcal{C}_i :

$$\mathcal{L}(\beta^2/2, \theta) = \prod_i P(\mathcal{O}_i | \mathcal{C}(i, \theta)). \quad (\text{A6})$$

This is easily extended to a fit that combines the SEP and DEP energy regions (index r),

$$\mathcal{L}(\beta^2/2, \theta) = \prod_r \prod_i P(\mathcal{O}_{ri} | \mathcal{C}_{ri}(i_r, \theta_r)). \quad (\text{A7})$$

Since the energies of the escape peaks are well known, we include a constraint on μ as a pull term to penalize any fit where μ deviates significantly from the expected value,

$$\mathcal{L}_{\text{pull}}(\mu) = \frac{1}{2\pi \sigma_{\text{res}}} e^{-\frac{\mu-\bar{\mu}}{\sigma_{\text{res}}}}. \quad (\text{A8})$$

The final binned likelihood used for our analysis is given by

$$\mathcal{L} = \mathcal{L}(\beta^2/2, \theta) \mathcal{L}_{\text{pull}}(\mu_r). \quad (\text{A9})$$

The best-fit values for our search are given in Table III.

Finding no significant signal in either echo peak region, we profile the likelihood function to set an upper limit on $\beta^2/2$. Nuisance parameters are fixed to their best-fit values, and the number of counts in the echo peak is increased until reaching a 95% CL upper limit. Fig. 6 expresses this profile over the likelihood function in terms of the $\beta^2/2$ parameter, for the SEP-only, DEP-only, and combined SEP+DEP analysis.

TABLE III. Best-fit parameters for the SEP and DEP calibration peaks.

Parameter	SEP	DEP
N_{peak} (counts)	33340	23300
μ (keV)	2103.5	1592.6
σ (keV)	1.92	1.20
f	0.133	0.14
τ (keV)	2.5	1.02
H (counts)	0	0
m (counts/keV)	0.31	2.47
n (counts)	210	-3240

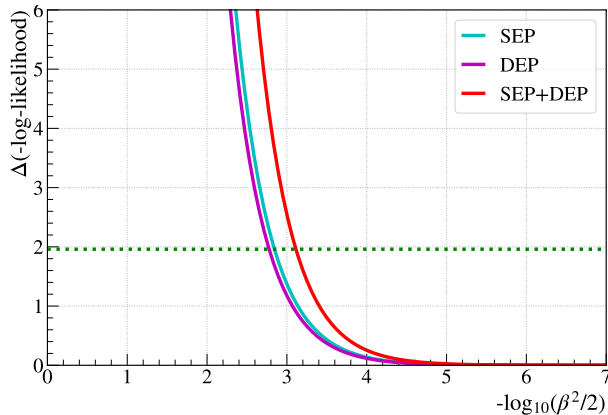


FIG. 6. $\Delta\log$ -likelihood as a function of $\beta^2/2$, used to set an upper limit to 95% CL (green horizontal line). The values are presented for SEP-only (cyan), DEP-only (purple), and SEP+DEP (red) methods. Higher values of $-\log_{10}(\beta^2/2)$ correspond to tighter upper limits.

Alternate analysis schemes exploiting the close-packed detector arrangement of the DEMONSTRATOR were also considered, including a technique of selecting only calibration events (multi-detector hits) where one detector records a 511 keV energy deposition, and searching for the same weak peaks alongside the DEP/SEP regions. For the MAJORANA data set, we find this method increases the signal-to-background (S/B) of the peaks by $\sim 15\%$ but lowers the overall number of events available for analysis by 66%. Near the SEP, we would require 1000 times more calibration data to make this method competitive, and the DEP requires another factor of 100 increase in statistics to provide similar results as the primary scheme of considering all available events.

^a Present address: SLAC National Accelerator Laboratory, Menlo Park, CA 94025, USA

^b inwookkim.physics@gmail.com; Present address: Lawrence Livermore National Laboratory, Livermore, CA 94550, USA

^c lopezcastajm@ornl.gov

^d Present address: Duke University, Durham, NC 27708, USA

^e wisecg@uw.edu

^f Present address: Jet Propulsion Laboratory, California Institute of Technology, Pasadena, CA 91109, USA

[1] C. S. Wu, E. Ambler, R. W. Hayward, D. D. Hoppes, and R. P. Hudson, *Phys. Rev.* **105**, 1413 (1957).

[2] S. J. Freedman and J. F. Clauser, *Phys. Rev. Lett.* **28**, 938 (1972).

[3] A. Aspect, J. Dalibard, and G. Roger, *Phys. Rev. Lett.* **49**, 1804 (1982).

[4] D. Bouwmeester, J.-W. Pan, K. Mattle, M. Eibl, H. Weinfurter, and A. Zeilinger, *Nature* **390**, 575 (1997).

[5] A. Y. Ignatiev and V. Kuzmin, *JETP Lett.* **47**, 6 (1987).

[6] O. W. Greenberg and R. N. Mohapatra, *Phys. Rev. Lett.* **59**, 2507 (1987).

[7] O. W. Greenberg, *Phys. Rev. D* **43**, 4111 (1991).

[8] O. W. Greenberg, in *AIP Conf. Proc.*, Vol. 545 (American Institute of Physics, 2000) pp. 113–127.

[9] R. Bernabei, P. Belli, F. Cappella, R. Cerulli, C. Dai, A. d’Angelo, H. He, A. Incicchitti, H. Kuang, X. Ma, *et al.*, *Eur. Phys. J C* **62**, 327 (2009).

[10] N. Abgrall *et al.*, *Eur. Phys. J C* **76**, 1 (2016).

[11] L. Okun and Y. Zeldovich, *Phys. Lett. B* **78**, 597 (1978).

[12] R. N. Mohapatra, *Phys. Rev. Lett.* **59**, 1510 (1987).

[13] J.-W. Chen, H.-C. Chi, S.-T. Lin, C.-P. Liu, L. Singh, H. T. Wong, C.-L. Wu, and C.-P. Wu, *Phys. Rev. D* **93**, 093012 (2016).

[14] C. E. Aalseth *et al.* (MAJORANA Collaboration), *Phys. Rev. Lett.* **120**, 132502 (2018).

[15] I. Arnquist *et al.* (MAJORANA Collaboration), arXiv:2207.07638 (2022), accepted to *Phys. Rev. Letters*.

[16] N. Abgrall *et al.*, *Phys. Rev. Lett.* **118**, 161801 (2017).

[17] I. Arnquist *et al.* (MAJORANA Collaboration), arXiv preprint arXiv:2206.10638 (2022).

[18] S. Alvis *et al.* (Majorana Collaboration), *Phys. Rev. Lett.* **120**, 211804 (2018).

[19] S. I. Alvis *et al.* (MAJORANA Collaboration), *Phys. Rev. D* **99**, 072004 (2019).

[20] I. J. Arnquist *et al.* (MAJORANA Collaboration), *Phys. Rev. Lett.* **129**, 080401 (2022).

[21] R. Workman, *Prog. Theor. Exp. Phys.* **2022**, 083C01 (2022).

- [22] P. Belli, R. Bernabei, C. Dai, H. He, G. Ignesti, A. Incicchitti, H. Kuang, J. Ma, F. Montecchia, O. Ponkratenko, *et al.*, *Phys. Lett. B* **460**, 236 (1999).
- [23] E. Noether, *Gott. Nachr.* **1918**, 235 (1918).
- [24] E. Witten, *Nature Physics* **14**, 116 (2018).
- [25] S.-Y. Chu, *Mod. Phys. Lett. A* **11**, 2251 (1996).
- [26] A. Ignatiev, V. Kuzmin, and M. Shaposhnikov, *Phys. Lett. B* **84**, 315 (1979).
- [27] S. L. Dubovsky, V. A. Rubakov, and P. G. Tinyakov, *Journal of High Energy Physics* **2000**, 041 (2000).
- [28] M. Agostini, S. Appel, G. Bellini, J. Benziger, D. Bick, G. Bonfini, D. Bravo, B. Caccianiga, F. Calaprice, A. Caminata, *et al.*, *Phys. Rev. Lett.* **115**, 231802 (2015).
- [29] W. Pauli, *Zeitschrift für Physik* **31**, 765 (1925).
- [30] S. Weinberg, *Phys. Rev.* **133**, B1318 (1964).
- [31] Y. Suzuki *et al.*, *Phys. Lett. B* **311**, 357 (1993).
- [32] R. Bernabei *et al.*, *Phys. Lett. B* **408**, 439 (1997).
- [33] G. Bellini *et al.* (Borexino Collaboration), *Phys. Rev. C* **81**, 034317 (2010).
- [34] C. Curceanu *et al.*, *Entropy* **19** (2017), 10.3390/e19070300.
- [35] A. Messiah and O. Greenberg, *Phys. Rev.* **136**, B248 (1964).
- [36] O. W. Greenberg and R. N. Mohapatra, *Phys. Rev. D* **39**, 2032 (1989).
- [37] K. Akama, H. Terazawa, and M. Yasuè, *Phys. Rev. Lett.* **68**, 1826 (1992).
- [38] A. Addazi and A. Marcianò, *International Journal of Modern Physics A* **35**, 2042003 (2020).
- [39] S. Elliott, B. LaRoque, V. Gehman, M. Kidd, and M. Chen, *Foundations of Physics* **42**, 1015 (2012).
- [40] K. Piscicchia, J. Marton, S. Bartalucci, M. Bazzi, S. Bertolucci, M. Bragadireanu, M. Cargnelli, A. Clozza, R. Del Grande, L. De Paolis, *et al.*, *Entropy* **22**, 1195 (2020).
- [41] F. Napolitano, S. Bartalucci, S. Bertolucci, M. Bazzi, M. Bragadireanu, C. Capocchia, M. Cargnelli, A. Clozza, L. De Paolis, R. Del Grande, *et al.*, *Symmetry* **14**, 893 (2022).
- [42] V. Gavrin, A. Y. Ignatiev, and V. Kuzmin, *Phys. Lett. B* **206**, 343 (1988).
- [43] S. I. Alvis *et al.* (MAJORANA Collaboration), *Phys. Rev. C* **100**, 025501 (2019).
- [44] N. Abgrall *et al.* (LEGEND Collaboration), arXiv preprint arXiv:2107.11462 (2021).
- [45] N. Abgrall *et al.* (MAJORANA Collaboration), *Adv. High Energy P* **2014**, 365432 (2014).
- [46] N. Abgrall *et al.* (MAJORANA Collaboration), *NIM A* **828**, 22 (2016).
- [47] N. Abgrall *et al.* (MAJORANA Collaboration), *NIM A* **872**, 16 (2017).
- [48] S. S. Wilks, *The annals of mathematical statistics* **9**, 60 (1938).
- [49] W. A. Rolke, A. M. López, and J. Conrad, *NIM A* **551**, 493 (2005).
- [50] F. James, *Statistical methods in experimental physics* (World Scientific Publishing Company, 2006).
- [51] C. Wiseman, *Journal of Physics: Conference Series* **1468**, 012040 (2020).